The N-terminal domain of TET1 promotes the formation of dense chromatin regions refractory to transcription

Audrey Lejart, Siham Zentout, Catherine Chapuis, Ostiane D'augustin, Rebecca Smith, Gilles Salbert, Sébastien Huet

The N-terminal domain of TET1 promotes the formation of dense chromatin regions refractory to transcription

Audrey Lejart[1], Siham Zentout[1], Catherine Chapuis[1], Ostiane D'Augustin[1,2], Rebecca Smith[1], Gilles Salbert[1,#] and Sébastien Huet[1,3#]

1 Univ Rennes, CNRS, IGDR (Institut de Génétique et Développement de Rennes) - UMR 6290, BIOSIT (Biologie, Santé, Innovation Technologique de Rennes) - UMS 3480, US 018, F-35000 Rennes, France
2 Institut de Biologie François Jacob, Institute of Cellular and Molecular Radiobiology, Université Paris-Saclay, Université de Paris, CEA, F-92265, Fontenay-aux-Roses, France.
3 Institut Universitaire de France, Paris, France

[#]Correspondence:
G.S. : Tel: +33 2 23 23 66 25; Email: gilles.salbert@univ-rennes1.fr
S.H. : Tel: +33 2 23 23 45 57; Email: sebastien.huet@univ-rennes1.fr

ABSTRACT

TET (Ten-eleven translocation) enzymes initiate active cytosine demethylation via the oxidation of 5-methylcytosine. TET1 is composed of a C-terminal domain, which bears the catalytic activity of the enzyme, and a N-terminal region that is less well characterized except for the CXXC domain responsible for the targeting to CpG islands. While cytosine demethylation induced by TET1 promotes transcription, this protein also interacts with chromatin regulating factors that rather silence this process, the coordination between these two opposite functions of TET1 being unclear. In the present work, we uncover a new function of the N-terminal part of the TET1 protein in the regulation of the chromatin architecture. This domain of the protein promotes the establishment of a compact chromatin architecture displaying reduced exchange rate of core histones and partial dissociation of the histone linker. This chromatin reorganisation process, which does not rely on the CXXC domain, is associated with a global shut-down of transcription and an increase in heterochromatin associated histone epigenetic marks. Based on these findings, we propose that the dense chromatin organisation generated by the N-terminal domain of TET1 could contribute in restraining the transcription enhancement induced by the DNA demethylation activity of this enzyme.

KEYWORDS

Ten eleven translocation enzyme, DNA methylation, DNA hydroxymethylation, chromatin, transcription, fluorescence microscopy.

INTRODUCTION

In the nucleus of eukaryotic cells, DNA is wrapped around histones to form the chromatin fibre which, itself, displays a hierarchy of folding steps. The complex organization of chromatin is essential to ensure that the entire genetic material of the cell can be contained within the nucleus, where it occupies 20 to 50% of the nuclear volume (Ou et al., 2017). Despite this high level of packaging, the chromatin structure is not fixed and constantly evolves in relation to multiple cellular processes which require access to DNA such as transcription, replication or repair (Fierz and Poirier, 2019). Key actors in the regulation of chromatin folding are epigenetic marks such as post-transcriptional modifications found on histones and base modifications found in DNA. These dynamic marks attract or repel effectors of DNA transactions and control chromatin organisation either directly, by modulating for example nucleosome stability, or indirectly, by recruiting remodelers or chromatin scaffolding proteins (Talbert and Henikoff, 2017).

While epigenetic marks found on histones are extremely diverse, only a handful of modifications are found at the DNA level, the main one being 5-methylcytosine (5-mC) (Raush et al., 2019). This mark, mainly found at CpG dinucleotides, has a repressive impact on transcription, in particular through the recruitment of repressor complexes and by regulating the binding of transcription factors to DNA at regulatory regions (Watt and Molloy, 1988; Iguchi-Ariga and Schaffner, 1989). 5-mC is written by several DNA methyl-transferase enzymes and its removal arises either by passive dilution due to DNA replication or by active DNA demethylation (Bhutani et al., 2011; Mulholland et al., 2020). The main active demethylation pathway is based on the successive oxidation of 5-mC into 5-hmC (5-hydroxymethylcytosine), 5-fC (5-formylcytosine) and finally 5-caC (5-carboxylcytosine), which are carried out by members of the TET (ten-eleven translocation) enzyme family (Ito et al., 2011). While the 5-fC and 5-caC forms are rapidly excised by the DNA repair machinery to restore an unmethylated cytosine (Maiti et al., 2011), 5-hmC has a relatively long lifetime and could thus constitute a fully-fledged epigenetic mark (Münzel et al., 2011).

The TET family is composed of three members showing distinct expression patterns hinting at different cellular functions (Lorsbach et al., 2003). All members share a catalytic domain responsible for 5-mC oxidation that is localized at the C-terminus of the proteins (Tahiliani et al., 2009; Hu et al., 2013). Furthermore, TET1 and TET3, but not TET2, bear a CXXC domain that binds to unmethylated CpGs and is thought to be responsible for the localization of these proteins at CpG-rich genomic sites like CpG islands, protecting them from aberrant methylation (Tahiliani et al., 2009). By controlling the balance of 5-mC/5-hmC levels within the genome, the TET enzymes are key regulators of transcriptional processes associated with cell differentiation, tumorigenesis and neurodegeneration (Rasmussen and Helin, 2016; Jin et al., 2016). However, the role of TET

enzymes is not limited to their catalytic activity. Indeed, they have been shown to serve as a binding platform for effectors that regulate transcription such as the histone methyltransferase complex PRC2 (Wu et al., 2011), the histone acetyltransferase hMOF (Zhong et al., 2017) or the O-linked N-acetylglucosamine transferase OGT (Shi et al., 2013; Bauer et al., 2015). Importantly, the existence of a shorter isoform of TET1 (TET1$_{short}$) has been recently reported. While the long isoform of TET1 (TET1$_{long}$) is expressed mainly in undifferentiated cells, TET1$_{short}$ levels seem to increase upon differentiation as well as during tumorigenesis (Zhang et al., 2016; Good et al., 2017). Despite lacking the N-terminal domain of TET1$_{long}$, including the CXXC domain, TET1$_{short}$ is still able to demethylate CpG islands (Zhang et al., 2016). Nevertheless, TET1$_{short}$ cannot fully complement the longer isoform, suggesting that the N-terminal domain of the full-length protein fulfils specific cellular functions that remain to be clarified.

In the present work, we demonstrate that the N-terminal region of the TET1 protein, which is lacking in TET1$_{short}$, is able to induce a global reorganisation of chromatin in three different human cell lines (U2OS, HeLa and MCF-7). This restructuring process is seen at the larger chromatin folding scales but also at the molecular level since histone exchange rates are impacted by the TET1 N-terminal domain. We also show that the chromatin reorganisation is associated with a global shut-down of transcription. Altogether, our findings uncover a previously unidentified function of TET1 in the regulation of the chromatin structure with potential consequences regarding its roles in the regulation of transcription.

RESULTS

Overexpression of TET1 leads to a global reorganisation of the chromatin structure

By using confocal fluorescence imaging, we observed that overexpression of GFP-TET1 and GFP-TET2, but not GFP-TET3, led to a global reorganisation of the chromatin within the nucleus of human osteosarcoma U2OS cells as seen both by Hoechst and anti-DNA staining (Fig. 1a and S1a). While the chromatin in control cells occupied the entire nuclear space relatively evenly, the expression of GFP-TET1 and GFP-TET2 led to chromatin condensation into large bundles, leaving some nuclear areas largely devoid of staining. Since this phenotype was more pronounced for TET1, we focused on the impact of TET1 expression on chromatin structure. To better understand how chromatin reorganisation arises upon TET1 overexpression, we transiently transfected GFP-tagged TET1 or free GFP in U2OS cells stably expressing H2B-mCherry and monitored the progressive increase in the GFP fluorescence levels in parallel with changes in the fluorescence contrast of the chromatin pattern, providing a readout of the chromatin compaction state in living cells. While no significant change in the chromatin pattern was observed in cells expressing GFP (Fig. S1b,c), a rapid increase of the fluorescence contrast of H2B-mCherry was observed upon

expression of GFP-TET1 (Fig. 1b,c). The tight correlation between the timing of the chromatin reorganisation and the rising of TET1 levels within the nucleus suggests that the change in the chromatin pattern is directly linked to the presence of TET1 rather than a secondary consequence of cellular mechanisms controlled by this enzyme.

TET1 is responsible for 5-mC oxidation to allow its later replacement by unmethylated cytosine (Tahiliani et al., 2009). However, when expressing a catalytically inactive form of TET1 we observed the same chromatin pattern as with the active enzyme (Fig. 1d). Furthermore, this reorganisation phenotype also did not rely on the CXXC domain of TET1 (Fig. 1d). Therefore, these data show that the change in chromatin structure promoted by TET1 is not the consequence of 5-mC oxidation processes or further DNA demethylation steps.

The N-terminal domain of TET1 is sufficient to induce chromatin reorganisation

To better delineate the domains of TET1 responsible for chromatin reorganisation, we analyzed the impact of the expression of two truncated forms of the full-length protein: a C-terminal fragment (CTER) bearing the catalytic domain shared between the different TET proteins, and a N-terminal fragment (NTER) which remains poorly characterized except for the CXXC domain (Fig 2a). Importantly, the CTER is reminiscent of the recently identified short isoform of TET1 found expressed in differentiated cells. While the CTER is still able to oxidize 5-mC into 5-hmC (Fig S2a,b), in line with what is reported for TET1$_{short}$ (Good et al., 2017), its expression in U2OS cells did not lead to visible changes in the chromatin organisation (Fig 2b). In contrast, expression of the NTER fragment, while not affecting 5-hmC levels within the nucleus (Fig S2a,b), led to a global reorganisation of the chromatin resembling the one observed when overexpressing the full-length protein (Fig 2b). The amount of chromatin reorganisation, assessed by the fluorescence contrast of the Hoechst staining, correlated with the levels of expression of the NTER fragment of TET1, similar to what was observed for the full-length protein (Fig S2c). Importantly, this chromatin restructuring phenotype upon expression of the NTER fragment was also observed in human HeLa and MCF-7 cells, demonstrating that it is not specific to U2OS cells (Fig 2c).

We also assessed the affinity of these two truncated TET1 constructs for chromatin by monitoring the kinetics of fluorescence recovery after photobleaching (FRAP) for each GFP tagged construct. The NTER fragment displayed a much slower recovery than the CTER construct (Fig 2d-f), in agreement with previous findings showing that it is principally the NTER region that controls TET1 binding to chromatin (Zhang et al., 2016). Nevertheless, the NTER fragment appeared less bound to chromatin than the full length TET1, which was also confirmed by a reduced colocalization of the former with Hoechst (Fig S2d). Altogether, these results demonstrate that the dynamic association of the N-terminal domain of TET1 with chromatin, which displays characteristic exchange times of

about 10 seconds, alters higher-order chromatin states, as shown by light microscopy, ultimately leading to a spatial redistribution of the genomic material within the nucleus.

Large-scale chromatin reorganisation promoted by the N-terminal domain of TET1 is associated with changes in histone association with chromatin

We next assessed whether the changes in chromatin folding induced by the N-terminal domain of TET1 were also associated with altered dynamics of its molecular constituents. Histones are key chromatin scaffolding proteins regulating the spatial organization of the genome within the nucleus, and their exchange rates correlate with the chromatin compaction state (Misteli et al., 2000; Bancaud et al., 2009). Therefore, we assessed the impact of the N-terminal domain of TET1 on the exchange rates of two different histones: the core histone H2B as well as the linker histone H1. Using FRAP, we observed that expression of the N-terminal domain of TET1 decreased H2B exchange rate (Fig 3a,b), in line with the fact that this domain seems to promote the local condensation of chromatin. Conversely, the linker histone H1 displayed reduced association with chromatin in cells expressing the N-terminal domain of TET1 compared to controls (Fig. 3c,d). Therefore, the dense chromatin domains generated by the expression of the N-terminal domain of TET1 differ from transcriptionally silent heterochromatic areas in which H1 displays increased binding (Misteli et al., 2000; Bancaud et al., 2009).

Expression of the N-terminal domain of TET1 leads to a global shutdown of transcription

The results obtained so far demonstrate that the N-terminal domain of TET1 regulates the architecture of chromatin at multiple scales. Since this enzyme was shown to play key roles in the regulation of transcription, we next tested whether the changes in chromatin organisation induced by the N-terminal domain of TET1 were also associated with a modulation of the transcriptional state. By quantifying 5-ethynyl uridine (EU) staining both by confocal imaging and flow cytometry to assess the level of nascent RNA in cells expressing the N-terminal domain of TET1, we found that the presence of this domain of TET1 led to a partial inhibition of transcription, similarly to the overexpression of the full-length protein (Fig. 4a-c and S3b). Furthermore, the negative colocalization between the EU and Hoechst staining in cells expressing the N-terminal domain of TET1 suggests that transcription is confined at the interface between the dense chromatin domains and the nucleoplasm (Fig. S3a). Concomitant to the reduction in RNA synthesis rates, immunofluorescence staining also showed that the expression of the N-terminal domain of TET1 increased the levels of trimethylation of the lysine 27 of histone H3 (H3K27me3) (Fig 4d-e), an epigenetic mark written by the PRC2 complex and found within facultative heterochromatin (Cao et al., 2002). These results were confirmed by flow cytometry, which also revealed a positive

correlation between the amount the N-terminal domain of TET1 expressed in the cells and the levels of H3K27me3 mark (Fig. 4f and S3b). Altogether, these findings demonstrate that the N-terminal domain of TET1 is able to shut-down transcription by establishing a chromatin environment displaying some of the characteristics found in heterochromatin regions.

DISCUSSION

Our data show that overexpression of TET1 promotes chromatin remodeling in three different human cell lines (U2OS, MCF-7 and HeLa), which leads to the establishment of a condensed chromatin architecture refractory to transcription. These dense chromatin domains observed in the presence of TET1 share some features found in heterochromatin, such as increased levels of H3K27me3 (Wiles and Selker, 2017), but nevertheless differ from these compact regions. Indeed, while the histone linker H1 was shown to be crucial for the condensation of the chromatin fiber (Willcockson et al., 2021), we observed reduced association of this histone in the compact chromatin conformation promoted by TET1. Interestingly, senescence associated heterochromatin foci, which arise from heterochromatic areas detaching from the nuclear lamina, also show reduced H1 binding due to its replacement by the high mobility group protein A2 (HMGA2) (Funayama et al., 2006). It would be useful to assess whether TET1 overexpression could promote cell senescence.

The TET1-mediated chromatin condensation process reported here is independent of both the catalytic activity of this enzyme and its targeting to CpG islands via the CXXC domain. The N-terminal region of the protein, which triggers this condensation, displays a strong affinity for chromatin. Therefore, it could serve as a platform to recruit factors modulating chromatin conformation, as it was recently proposed for OGT (Zhang et al., 2016). TET1 has been shown to interact with the histone-deacetylases Sin3A and HDAC1 as well as the chromatin remodeler CHD4, three actors known to promote chromatin compaction (Shi et al., 2013). Future experiments would be needed to assess whether the recruitment of these proteins to chromatin through their binding to TET1 could contribute to the establishment of the compact genome organisation observed in cells expressing the N-terminal domain of TET1. Furthermore, the increase in H3K27me3 staining in these dense domains may be promoted by the association between TET1 and the PRC2 complex (Neri et al., 2015), contributing to a global silencing of transcription.

In this work, we uncovered a new role of the N-terminal region of TET1 in the regulation of the chromatin organisation and transcription inhibition. The inhibitory impact of this region of the protein might be needed to balance the positive influence of the catalytic domain on transcription, where unrestrained activity of the recently identified short isoform of TET1 is associated with

tumorigenesis (Good et al., 2017). Further work will be needed to better delineate the characteristics of this coordination mechanism between the two domains of TET1.

METHODS

Plasmids

Plasmids coding for the full length TET1, TET2 and TET3 tagged with GFP on their N-terminal end are gifts from Heinrich Leonhardt and Cristina Cardoso (Frauer et al., 2011). The plasmids coding for the C-terminal and N-terminal fragments of TET1, both tagged with GFP on their C-terminal end, as well as the TET1 mutant lacking the CXXC domain, tagged with GFP on its N-terminal end, were provided by Wei Xie (Zhang et al., 2016). The catalytically-inactive mutant of full length TET1 fused to GFP on its N-terminal end was obtain by site-directed mutagenesis on GFP tagged TET1 with primers 5'- gttgtgcatgttgtgaatggccttgtaagaatgggcacaaaaatcc-3' and 5'-ggatttttgtgcccattcttacaaggccattcacaacatgcacaac-3' using Phusion polymerase (Thermo Scientific). Haico Van Attikum (Rother et al., 2020) provided the plasmid coding for GFP fused to a NLS (nuclear localisation sequence), which promotes GFP accumulation in the nucleus.The H2B-mCherry was a gift from Jan Ellenberg (Euroscarf P30632, (Neumann et al., 2010)). mEGFP was cut from H1-mEGFP (gift from Gyula Timinszky) and replaced with mCherry using the restriction sites BshTI and Bsp1407I (ThermoScientific), to generate the H1-mCherry construct.

Cell culture

The experiments were performed on three different human cell lines: osteosarcoma U2OS cells, cervical carcinoma HeLa cells and breast cancer MCF-7 cells. All cell lines were cultured in DMEM (4.5 g/L glucose, Sigma) supplemented with 10% fetal bovine serum (Life Technologies), 2 mM glutamine (Sigma), 100 µg/mL penicillin and 100 U/mL streptomycin (Sigma) in a humidified incubator at 37 °C with 5% CO_2. For transient expression of fluorescent constructs, cells were transfected 5 hours after seeding into glass-bottom chambers (Thermo Scientific and Zell Contact) with XtremeGENE HP (Roche) or Xfect (Takara Bio) according to the manufacturer's instructions. U2OS stably expressing H2B-mCherry were generated by transfection of the H2B-mCherry plasmid followed by a two-week selection in growing medium supplemented with puromycin (0.25µg/ml, Invivogen). Immediately prior to imaging live cells, growth medium was replaced with CO_2-independent imaging medium (Phenol Red-free Leibovitz's L-15 medium (Life Technologies) supplemented with 20% fetal bovine serum, 2 mM glutamine, 100 µg/mL penicillin and 100 U/mL streptomycin). All experiments were completed with unsynchronized cells.

Immunofluorescence staining

Cells were fixed using 4% paraformaldehyde and permeabilized with 0.1% Triton X-100 at room temperature. For 5-hmC staining, chromatin was denaturated by adding hydrochloric acid at 2 M for 30min. Cells were blocked with blocking buffer (BSA 3% Tween 0.05% in PBS) before incubation overnight at 4°C with primary antibodies recognizing double-strand DNA (Abcam, ab27156), 5-hmC (Active Motif, ref 39769) or the trimethylation of histone H3 at lysine 27 (Upstate, ref 07-449), diluted in the blocking buffer. The secondary antibodies labeled with Alexa Fluor 555 (ThermoScientific, ref A21428) diluted in blocking buffer was added for one hour at room temperature. DNA was stained for 15 min with Hoechst 33342 at 1µg/mL (ThermoScientific).

Nascent RNA staining by 5-ethynyl uridine

For nascent RNA staining, cells were incubated with 5-ethynyl uridine (EU) at 1 mM in culture medium for 1 h before being fixed with 4% paraformaldehyde. Cells were permeabilised with 0.1% Triton X-100 for 15 min before RNA was labeled using the Click-iT® RNA Alexa Fluor 594 Imaging Kit according to the manufacturer's instructions (ThermoScientific).

Confocal imaging and fluorescence recovery after photobleaching

Fluorescence imaging of live and fixed cells was on a LSM880 point-scanner confocal microscope (Zeiss) using a 60x/1.4 N.A. oil-immersion objective lens. The pinhole was set to one Airy unit and fluorescence detection was performed on a GaAsP detector array. The fluorescence of the Hoechst was excited at 405 nm and detected within a window ranging from 415 to 470 nm. The fluorescence of the GFP was excited at 488 nm and detected within a window ranging from 500 to 550 nm. The fluorescence of the mCherry and Alexa Fluor 555 was excited at 561 nm and detected within a window ranging from 580 to 650 nm. The fluorescence of the Alexa Fluor 594 was excited at 594 nm and detected within a window ranging from 605 to 695 nm. The pixel size was set to 70 nm. Laser intensities and detector gains were chosen to avoid detector saturation and the acquisition settings were kept constant within the course of a given experiment. FRAP of H2B-mCherry was performed on the same setup. Photobleaching was achieved by 30 iterations of scanning half the nucleus at 100% power of the 561 nm laser. Then cells were imaged for 11 h at 1 image per hour to monitor the progressive recovery within the bleached area. FRAP of H1-mCherry as well as the full-length or truncated forms of TET1 tagged with GFP was completed on a Ti-E inverted microscope from Nikon equipped with a CSU-X1 spinning-disk head from Yokogawa, a Plan APO 60x/1.4 N.A. oil-immersion objective lens and a sCMOS ORCA Flash 4.0 camera. A 4 µm diameter circle within the nucleus was bleached by 40 consecutive scans at 100% of 561 or 488 nm and subsequent fluorescence recovery was monitored by imaging the cells for 25 to 50 seconds at 4 frames/second. For all live-cell experiments, cells were maintained at 37°C with a heating chamber.

Image analysis

Image analysis was performed using the ImageJ software. For the quantification of fluorescence signals, the mean intensity within manually defined region delineating the nucleus was measured and subtracted from background. Colocalization between two channels was performed by calculating the Pearson coefficient using the JACoP plugin (Bolte et al., 2006). To assess chromatin compaction, we estimated the fluorescence contrast on images of nuclei expressing H2B-mCherry or stained with Hoechst, using the plugin GLCM_Texture written by Julio E. Cabrera. The contrast is one of the Haralick features (Haralick et al., 1973) and measures the mean squared intensity difference between pixels separated by a given distance *d*. This distance *d* was set to 10 pixels, which corresponded to the characteristic size of the dense chromatin domains generated by TET1 overexpression. Since we found that the measured contrast was independent of the cardinal directions, this parameter was only calculated along the east direction. The contrast estimated for each nucleus was the average of the values measured for three regions of 20*20 pixels randomly chosen within this nucleus, taking care that these regions do not overlap with the nucleus border or the nucleoli. For the timelapse acquisitions shown on figures 1b and S1b the changes in fluorescence contrast were measured from the images of the H2B-mCherry patterns and the levels of expression of unfused GFP or GFP-TET1 was assessed by the mean intensity in the GFP channel. The expression level was then rescaled to range between 0 and 1. Before averaging, the individual curves for the chromatin contrast and the expression level were aligned in time using as a reference the timepoint at which the normalized expression level equalled 0.5. The time was then estimated relative to this reference timepoint.

To analyze the FRAP acquisitions, regions of interest were defined manually to measure the fluorescence intensities within the bleached area (I_{bleach}), the whole nucleus (I_{nuc}) and outside the cell (I_{bg}), along the entire image sequence. Based on these intensity measurements, the intensity within the bleached area was corrected from background and from the loss of total nuclear intensity due to both local photobleaching and timelapse imaging (Bancaud et al., 2010), using the following expression:

$$I_{frap} = \frac{I_{bleach} - I_{bg}}{I_{nuc} - I_{bg}}$$

After subtracting the signal estimated immediately after the bleach, the intensity was normalized to the pre-bleach signal. To estimate the characteristic recovery time, the post-bleach curves were fitted with the following single exponential recovery model:

$$I_{rec}(t) = 1 - \exp(-t/\tau),$$

with t the time after bleaching and τ the fitted characteristic recovery time.

Flow cytometry

For staining with the Click-iT® RNA reagent (ThermoScientific), U2OS cells were seeded into 6-well plates and transfected with the corresponding GFP tagged TET1 expression plasmid. After 16h, cells were treated for 1h at 37°C with 1mM of 5-ethynyl uridine diluted in DMEM medium. Then, cells were harvested by trypsinization and fixed with 4% paraformaldehyde for 20min at room temperature. After permeabilization for 15 min using the Click-iT® saponin-based permeabilization reagent, the cells were stained with the click-chemistry cocktail according to the manufacturer's instructions for 30 min at room temperature and protected from light. For H3K27me3 staining, U2OS cells were seeded into 6-well plates and transfected with the corresponding GFP tagged TET1 expression plasmid. After 16 h, cells were fixed with 4% paraformaldehyde, permeabilized with saponin-based permeabilization reagent and incubated with rabbit polyclonal antibody against H3K27me3 (Sigma-Aldrich, 07-449) for 1 h at 1/100 dilution in the permeabilization reagent. After three cycles of washes/centrifugation with the permeabilization buffer, the pellet was resuspended and stained for 30 min using a 1/1000 dilution of Alexa Fluor 647 secondary antibody (ThermoScientific, A315573). Finally, the samples were washed/centrifuged three times with PBS and the pellets were resuspended with PBS for cytometry analysis.

All the conditions were analyzed on a LSRFortessa X-20 (BD Bioscience) using BD FACSDiva Software v8.0.1. GFP was excited at 488nm laser and detected within 30 nm window centred on 530 nm. For the Click-iT® staining using Alexa Fluor 594, fluorescence was excited with a 575nm laser and detected within a 30 nm window centred on 620 nm. Alexa Fluor-647 was excited at 640 nm laser and detected within a 30 nm window centred on 670 nm. At least 10^5 events were collected for each condition. Quantifications were performed with the FACSDiva software (BD Biosciences).

Statistics

All the experiments were performed in at least three replicates with reproducible results for each replicate. When a single experiment is shown, a typical replicate was chosen. For the curves displaying time courses, means±SD are shown. Boxplots were generated using a web-tool developed by the Tyers and Rappsilber labs (http://boxplot.tyerslab.com/). The box limits correspond to the 25th and 75th percentiles and the bold line indicates the median value. The whiskers extend 1.5 times the interquartile range and outliers are shown by dots. The numbers in parentheses below each condition refer to the number of cells, for the imaging data, or to the number of experiments, for the cytometry data. p values were calculated using either two-sided unpaired Student's t-test assuming unequal variances for data showing normal distributions, or

unpaired two-samples Wilcoxon test. On the boxplots, * refers to $p<0.05$, ** to $p<0.01$, *** to $p<0.001$, **** to $p<0.0001$ and n.s. to non significant.

DECLARATIONS

Ethics approval and consent to participate

Not applicable

Consent for publication

Not applicable

Availability of data and materials

The raw datasets used during the current study are available from the corresponding authors on reasonable request.

Code availability

Not applicable

Competing interests

The authors declare no competing interests.

Funding

This work was funded by the Ligue contre le Cancer du Grand-Ouest, the Conseil Régional de Bretagne and the Institut Universitaire de France. The Microscopy-Rennes Imaging Center (BIOSIT, Université Rennes 1), a member of the national infrastructure France-BioImaging supported by the French National Research Agency (ANR-10-INBS-04).

Authors' contributions

A.L., S.Z., S.H. and R.S. completed the experiments within the manuscript. C.C. generated cell lines and DNA constructs. A.L., S.Z., S.H. and O.D.A. performed data analysis. G.S. and S.H. conceived and supervised this study. S.H. wrote the manuscript. All authors read and commented on the manuscript.

Acknowledgements

We thank the engineers of the Microscopy Rennes Imaging Center (BIOSIT, Université Rennes 1), Stéphanie Dutertre and Xavier Pinson for technical help on the microscopes. We are also grateful to the engineers of the flow cytometry facility (BIOSIT, Université Rennes 1), Laurent Deleurme and Alexis Aimé for technical assistance. This work would not have been possible without the generous donation of plasmids from Heinrich Leonhardt, Cristina Cardoso, Wei Xie, Haico Van Attikum, Gyula Timinszky and Jan Ellenberg.

REFERENCES

Bancaud A, Huet S, Daigle N, et al (2009) Molecular crowding affects diffusion and binding of nuclear proteins in heterochromatin and reveals the fractal organization of chromatin. EMBO J 28:3785–3798. https://doi.org/10.1038/emboj.2009.340

Bancaud A, Huet S, Rabut G, Ellenberg J (2010) Fluorescence perturbation techniques to study mobility and molecular dynamics of proteins in live cells: FRAP, photoactivation, photoconversion, and FLIP. Cold Spring Harb Protoc 2010:pdb.top90. https://doi.org/10.1101/pdb.top90

Bauer C, Göbel K, Nagaraj N, et al (2015) Phosphorylation of TET Proteins Is Regulated via O-GlcNAcylation by the O-Linked N-Acetylglucosamine Transferase (OGT). Journal of Biological Chemistry 290:4801–4812. https://doi.org/10.1074/jbc.M114.605881

Bhutani N, Burns DM, Blau HM (2011) DNA demethylation dynamics. Cell 146:866–872. https://doi.org/10.1016/j.cell.2011.08.042

Bolte S, and Cordelieres FP (2006) A guided tour into subcellular colocalization analysis in light microscopy, J Microsc 224:213-232. https://doi: 10.1111/j.1365-2818.2006.01706.x

Cao R, Wang L, Wang H, et al (2002) Role of histone H3 lysine 27 methylation in Polycomb-group silencing. Science 298:1039–1043. https://doi.org/10.1126/science.1076997

Fierz B, Poirier MG (2019) Biophysics of Chromatin Dynamics. Annu Rev Biophys 48:321–345. https://doi.org/10.1146/annurev-biophys-070317-032847

Frauer C, Rottach A, Meilinger D, et al (2011) Different binding properties and function of CXXC zinc finger domains in Dnmt1 and Tet1. PLoS One 6:e16627. https://doi.org/10.1371/journal.pone.0016627

Funayama R, Saito M, Tanobe H, Ishikawa F (2006) Loss of linker histone H1 in cellular senescence. J Cell Biol 175:869–880. https://doi.org/10.1083/jcb.200604005

Good CR, Madzo J, Patel B, et al (2017) A novel isoform of TET1 that lacks a CXXC domain is overexpressed in cancer. Nucleic Acids Res 45:8269–8281. https://doi.org/10.1093/nar/gkx435

Haralick RM, Shanmugam K and Dinstein I (1973) Textural Features for Image Classification. IEEE Transactions on Systems, Man, and Cybernetics 3:610-621. https//doi.org/10.1109/TSMC.1973.4309314.

Hu L, Li Z, Cheng J, et al (2013) Crystal structure of TET2-DNA complex: insight into TET-mediated 5mC oxidation. Cell 155:1545–1555. https://doi.org/10.1016/j.cell.2013.11.020

Iguchi-Ariga SM, Schaffner W (1989) CpG methylation of the cAMP-responsive enhancer/promoter sequence TGACGTCA abolishes specific factor binding as well as transcriptional activation. Genes Dev 3:612–619. https://doi.org/10.1101/gad.3.5.612

Ito S, Shen L, Dai Q, et al (2011) Tet proteins can convert 5-methylcytosine to 5-formylcytosine and 5-carboxylcytosine. Science 333:1300–1303. https://doi.org/10.1126/science.1210597

Jin S-G, Zhang Z-M, Dunwell TL, et al (2016) Tet3 Reads 5-Carboxylcytosine through Its CXXC Domain and Is a Potential Guardian against Neurodegeneration. Cell Rep 14:493–505. https://doi.org/10.1016/j.celrep.2015.12.044

Lorsbach RB, Moore J, Mathew S, et al (2003) TET1, a member of a novel protein family, is fused to MLL in acute myeloid leukemia containing the t(10;11)(q22;q23). Leukemia 17:637–641. https://doi.org/10.1038/sj.leu.2402834

Maiti A, Drohat AC (2011) Thymine DNA glycosylase can rapidly excise 5-formylcytosine and 5-carboxylcytosine: potential implications for active demethylation of CpG sites. J Biol Chem 286:35334–35338. https://doi.org/10.1074/jbc.C111.284620

Misteli T, Gunjan A, Hock R, et al (2000) Dynamic binding of histone H1 to chromatin in living cells. Nature 408:877–881. https://doi.org/10.1038/35048610

Mulholland CB, Nishiyama A, Ryan J, et al (2020) Recent evolution of a TET-controlled and DPPA3/STELLA-driven pathway of passive DNA demethylation in mammals. Nat Commun 11:5972. https://doi.org/10.1038/s41467-020-19603-1

Münzel M, Globisch D, Carell T (2011) 5-Hydroxymethylcytosine, the sixth base of the genome. Angew Chem Int Ed Engl 50:6460–6468. https://doi.org/10.1002/anie.201101547

Neri F, Incarnato D, Krepelova A, et al (2015) TET1 is controlled by pluripotency-associated factors in ESCs and downmodulated by PRC2 in differentiated cells and tissues. Nucleic Acids Res 43:6814–6826. https://doi.org/10.1093/nar/gkv392

Neumann B, Walter T, Hériché J-K, et al (2010) Phenotypic profiling of the human genome by time-lapse microscopy reveals cell division genes. Nature 464:721–727. https://doi.org/10.1038/nature08869

Ou HD, Phan S, Deerinck TJ, et al (2017) ChromEMT: Visualizing 3D chromatin structure and compaction in interphase and mitotic cells. Science 357:. https://doi.org/10.1126/science.aag0025

Rasmussen KD, Helin K (2016) Role of TET enzymes in DNA methylation, development, and cancer. Genes Dev 30:733–750. https://doi.org/10.1101/gad.276568.115

Rausch C, Hastert FD, Cardoso MC (2019) DNA Modification Readers and Writers and Their Interplay. J Mol Biol. https://doi.org/10.1016/j.jmb.2019.12.018

Rother MB, Pellegrino S, Smith R, et al (2020) CHD7 and 53BP1 regulate distinct pathways for the re-ligation of DNA double-strand breaks. Nat Commun 11:5775. https://doi.org/10.1038/s41467-020-19502-5

Shi F-T, Kim H, Lu W, et al (2013) Ten-eleven translocation 1 (Tet1) is regulated by O-linked N-acetylglucosamine transferase (Ogt) for target gene repression in mouse embryonic stem cells. J Biol Chem 288:20776–20784. https://doi.org/10.1074/jbc.M113.460386

Tahiliani M, Koh KP, Shen Y, et al (2009) Conversion of 5-methylcytosine to 5-hydroxymethylcytosine in mammalian DNA by MLL partner TET1. Science 324:930–935. https://doi.org/10.1126/science.1170116

Talbert PB, Henikoff S (2017) Histone variants on the move: substrates for chromatin dynamics. Nature Reviews Molecular Cell Biology 18:115–126. https://doi.org/10.1038/nrm.2016.148

Watt F, Molloy PL (1988) Cytosine methylation prevents binding to DNA of a HeLa cell transcription factor required for optimal expression of the adenovirus major late promoter. Genes Dev 2:1136–1143. https://doi.org/10.1101/gad.2.9.1136

Wiles ET, Selker EU (2017) H3K27 methylation: a promiscuous repressive chromatin mark. Curr Opin Genet Dev 43:31–37. https://doi.org/10.1016/j.gde.2016.11.001

Willcockson MA, Healton SE, Weiss CN, et al (2021) H1 histones control the epigenetic landscape by local chromatin compaction. Nature 589:293–298. https://doi.org/10.1038/s41586-020-3032-z

Wu H, D'Alessio AC, Ito S, et al (2011) Dual functions of Tet1 in transcriptional regulation in mouse embryonic stem cells. Nature 473:389–393. https://doi.org/10.1038/nature09934

Zhang W, Xia W, Wang Q, et al (2016) Isoform Switch of TET1 Regulates DNA Demethylation and Mouse Development. Mol Cell 64:1062–1073. https://doi.org/10.1016/j.molcel.2016.10.030

Zhong J, Li X, Cai W, et al (2017) TET1 modulates H4K16 acetylation by controlling auto-acetylation of hMOF to affect gene regulation and DNA repair function. Nucleic Acids Res 45:672–684. https://doi.org/10.1093/nar/gkw919

FIGURE LEGENDS

Figure 1. The overexpression of GFP-TET1 leads to chromatin reorganisation. a. Images of Hoechst-stained UO2S cells expressing either unfused GFP, or GFP-tagged TET1, TET2 or TET3. Cells were imaged 24h after transfection. More than 30 cells were imaged per condition and a typical image is shown for each of them. **b.** Timelapse image sequence of live U2OS cells stably expressing H2B-mCherry and transiently expressing GFP-TET1. The images were pseudocolored according to the look-up table displayed below the images. The timelapse acquisition started 6 h after transfection **c.** Images from b. were quantified to monitor the changes in GFP-TET1 expression levels (black curve), assessed by GFP fluorescence intensity, in parallel to the chromatin spatial distribution, assessed by the fluorescence contrast estimated from the images of the H2B-mCherry signal (red curve). The curves show a mean ± SD of 17 cells. Before averaging, the individual curves for the chromatin contrast and the expression level were aligned in time using as a reference the timepoint at which the normalized expression level equalled 0.5. The time was then estimated relative to this reference timepoint. **d.** Images of Hoechst-stained U2OS cells expressing either unfused GFP, or full-lenght TET1 (GFP-FL), a catalytically-inactive mutant of TET1 (GFP-FLmut) or a TET1 construct lacking the CXXC domain (GFP-ΔCXXC), all tagged with GFP. Cells were imaged 24h after transfection. For panels a., b. and d., scale bars = 10 μm.

Figure 2. The N-terminal domain of TET1 promotes chromatin reorganisation. a. Schematic representation of the GFP-tagged TET1 protein domains. Cys-rich corresponds to a cysteine-rich region and DSBH stands for double-stranded β-helix. **b.** Images of Hoechst-labeled U2OS cells expressing either unfused GFP, full-length (GFP-FL), N-terminal domain (NTER-GFP) or C-terminal domain (CTER-GFP) of TET1, all tagged with GFP. More than 100 cells were imaged per condition and a typical image is shown for each. **c.** Images of Hoechst-labeled HeLa and MCF-7 cells expressing unfused GFP or the N-terminal of TET1 tagged with GFP. More than 30 cells were imaged per condition and a typical image is shown for each. **d.** Image sequences of the fluorescence redistribution after photobleaching a circular area of the nucleus (dotted red circles) of U2OS cells

expressing either GFP fused to a nuclear localisation sequence (GFP-NLS), full-length TET1 (GFP-FL), the N-terminal domain of the protein (NTER-GFP) or its C-terminal domain (CTER-GFP), all tagged with GFP. **e.** Image from d. were quantified to assess the fluorescence recovery within the bleached region. The curves show a mean ± SD of 15 to 20 cells for each condition. **f.** Characteristic recovery times estimated from the fitting of the curves shown on panel e. For all the data shown on this figure, cells were imaged 24 h after transfection. For panels b. to d., scale bars = 10 μm.

Figure 3. The N-terminal domain of TET1 affects the association of histones H2B and H1 with chromatin. a. Image sequences of the fluorescence recovery after photobleaching of the mCherry signal within half of the nucleus (dotted red outlines) of U2OS cells expressing H2B-mCherry together with either unfused GFP or the N-terminal domain of TET1 (NTER-GFP) tagged with GFP. **b.** Images from a. were quantified to assess the fluorescence recovery within the bleached region (left). The curves show a mean ± SD of 15 and 17 cells for the unfused GFP control and the NTER-GFP condition, respectively. The FRAP curves were then fitted with a single-exponential recovery model to extract the characteristic recovery times (right). **c.** Image sequences of the fluorescence recovery after photobleaching of the mCherry signal within a circular area of the nucleus (dotted red circles) of U2OS cells expressing H1-mCherry together with either unfused GFP or the N-terminal domain of the protein (NTER-GFP) tagged with GFP. **d.** Images from e. were quantified to assess the fluorescence recovery within the bleached region (left). The curves show a mean ± SD of 18 and 17 cells for the unfused GFP control and the NTER-GFP condition, respectively. The FRAP curves were then fitted with a single-exponential recovery model to extract the characteristic recovery times (right). For all the data shown on this figure, cells were imaged 24 h after transfection. For panels a. and c., scale bars = 10 μm.

Figure 4. The N-terminal domain of TET1 promotes transcription shut-down and H3K37me3 enrichment a. Images of Hoechst-stained U2OS cells expressing either unfused GFP, full-length (GFP-FL) or the N-terminal domain of TET1 (NTER-GFP), both tagged with GFP. The levels of nascent RNA were monitored by EU staining. More than 100 cells were imaged per condition and a typical image is shown for each. **b.** Images from a. were quantified to estimate the mean nuclear levels of EU staining in each condition. **c.** Quantification of EU signals measured by flow cytometry in U2OS cells transfected with full-length (GFP-FL) or the N-terminal domain of TET1 (NTER-GFP), both tagged with GFP. The EU signal measured in the cells expressing these two constructs was normalized against the one measured in the GFP negative cells (GFP-). The mean ± SEM of 6 independent experiments is shown. **d.** Images of Hoechst-stained U2OS cells expressing

either unfused GFP, full-length (GFP-FL) or the N-terminal domain of TET1 (NTER-GFP), both tagged with GFP. The cells were also immunostained for the H3K27me3 histone mark. More than 100 cells were imaged per condition and a typical image is shown for each. **e.** Images from d. were quantified to estimate the mean nuclear levels of H3K27me3 in each condition. **f.** Quantification of H3K27me3 signals measured by flow cytometry in U2OS cells transfected with full-length (GFP-FL) or the N-terminal domain of TET1 (NTER-GFP), both tagged with GFP. The H3K27me3 signal measured in the cells expressing these two constructs was normalized against the one measured in the GFP negative cells (GFP-). The mean ± SEM of 4 independent experiments is shown. For all the data shown on this figure, cells were fixed and stained 24 h after transfection. For panels a. and d., scale bars = 10 µm.

Supplementary Figure 1. Controls of the changes in chromatin compaction state upon expression of unfused GFP and GFP-TET1. a. Images of U2OS cells stained with Hoechst as well as an anti-dsDNA antibody, and expressing either unfused GFP (GFP) or full-length (GFP-TET1). Cells were fixed and stained 24 h after transfection. More than 30 cells were imaged per condition and a typical image is shown for each. **b.** Timelapse image sequence of live U2OS cells stably expressing H2B-mCherry and transiently expressing unfused GFP. The images were pseudocolored according to the look-up table displayed below the images. The timelapse acquisition started 6 h after transfection **c.** Images from a. were quantified to monitor the changes in GFP expression levels (black curve), assessed by GFP fluorescence intensity, in parallel to the chromatin spatial distribution, assessed by the fluorescence contrast estimated from the images of the H2B-mCherry signal (red curve). The curves show a mean ± SD of 11 cells. Before averaging, the individual curves for the chromatin contrast and the expression level were aligned in time using as a reference the timepoint at which the normalized expression level equalled 0.5. The time was then estimated relative to this reference timepoint. For panels a. and b., scale bars = 10 µm.

Supplementary Figure 2. Influence of the N-terminal and C-terminal domains of TET1 on the levels of 5-hmC and the chromatin patterns. a. Images of Hoechst-stained UO2S cells expressing either unfused GFP, full-length TET1 (GFP-FL), the C-terminal domain of TET1 (CTER-GFP) or the N-terminal domain of TET1 (NTER-GFP), all tagged with GFP. The cells were also immunostained for 5-hmC. Cells were fixed and stained 24 h after transfection. More than 30 cells were imaged per condition and a typical image is shown for each. Scale bars = 10 µm. **b.** Scatter plot of the mean nuclear intensity of the 5hmC staining plotted as a function of the mean nuclear signal in the GFP channel measured from the cells shown in a. **c.** Scatter plot of the fluorescence contrast, estimated from the Hoechst staining, plotted against the mean nuclear GFP signal

measured from the images of U2OS cells expressing GFP-tagged full-length or the N-terminal domain of TET1, which are shown on figure 2b. The correlation between the contrast and the GFP signal was estimated by calculating the Spearman coefficient. The dotted line correponds to the linear fit of the experimental points. **d.** The colocalisation between the Hoechst and GFP stainings in U2OS cells expressing GFP-tagged full-length or the N-terminal domain of TET1 was estimated by calculating the Pearson coefficient between the two channels on the images shown on figure 2a.

Supplementary Figure 3. Analysis of EU and H3K27me3 staining in cells expressing full-length or the N-terminal domain of TET1. a. The colocalization between the Hoechst and EU staining on the images shown on figure 4a was estimated by calculating the Pearson coefficient between the two channels **b.** Gating strategy for the analysis of EU and H3K27me3 staining by flow cytometry. The first gate was performed on the scatter plot of SSC-A against FSC-A to select living cells (right). The second gate was applied to the scatter plot of SSC-A against SSC-H to remove cell doublets (middle). Finally, the scatter plot of the EU or H3K27me3 signals against the GFP signal (FITC-A::GFP) was analyzed (left). Gates for cells negative for GFP (GFP-) or negative for EU or H3K27me3 staining were established based on the signals obtained for U2OS cells that were not subjected to transfection and EU or H3K27me3 staining. Finally, the GFP positive cells were divided into 3 equal subpopulations: low, medium and high expressing cells.

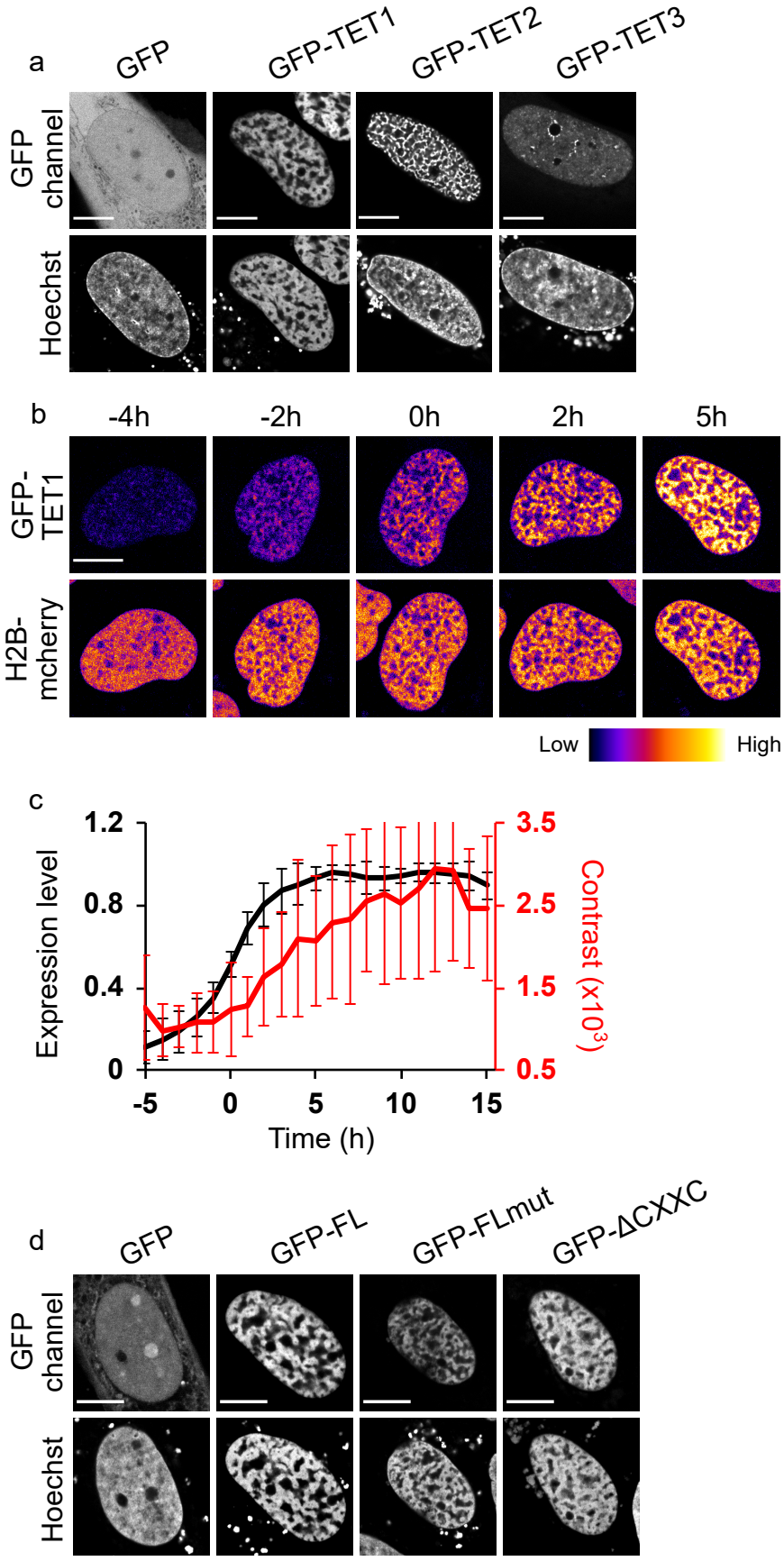

Lejart et al., Figure1.

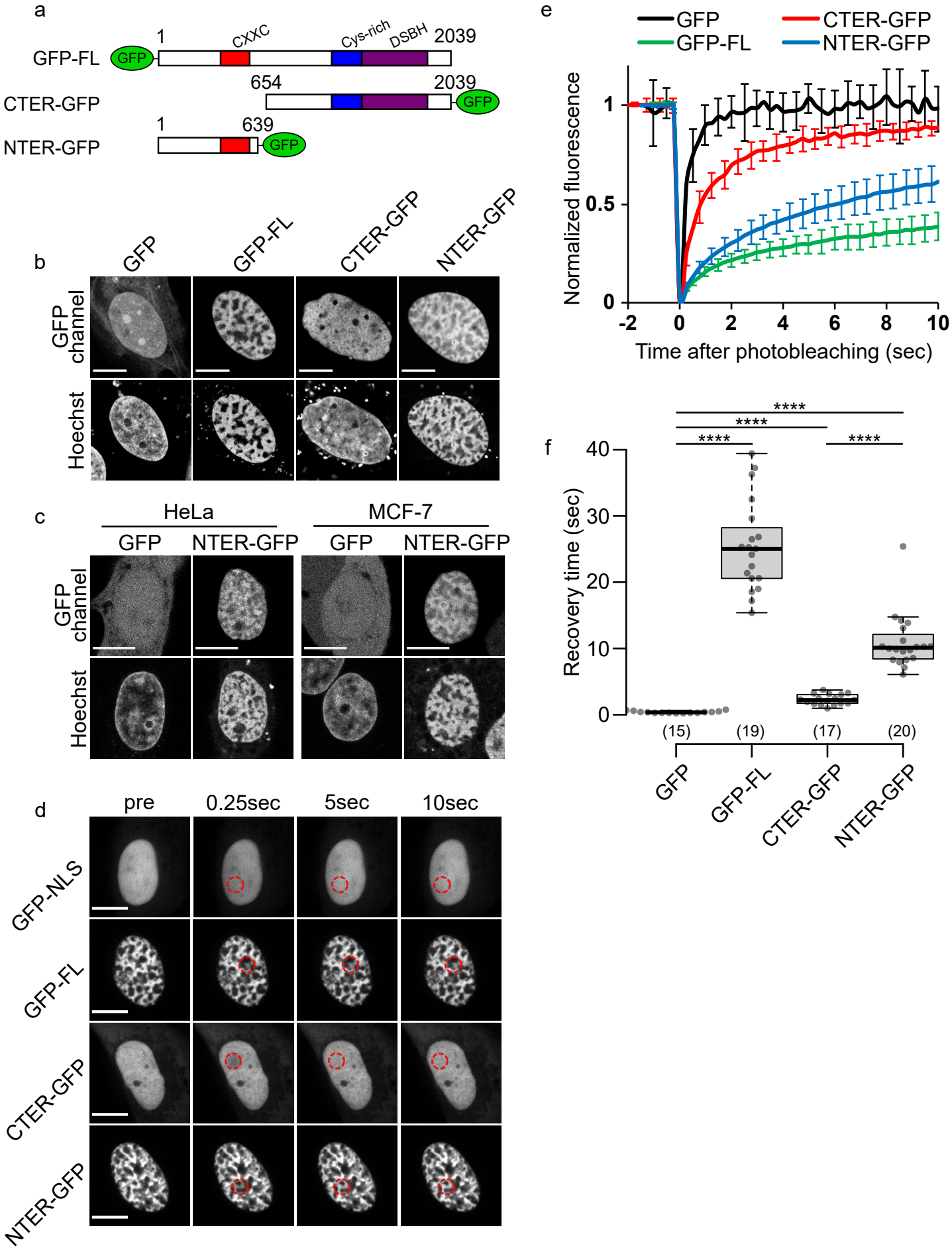

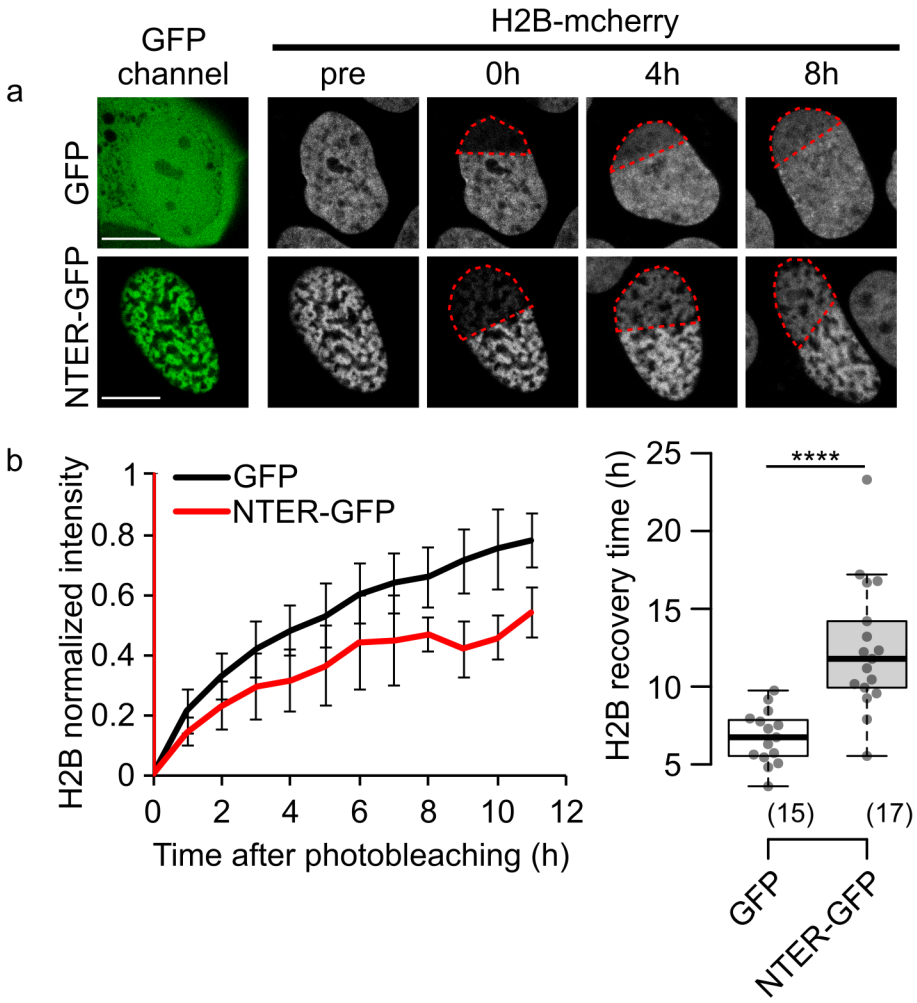

Lejart et al., Figure 3.

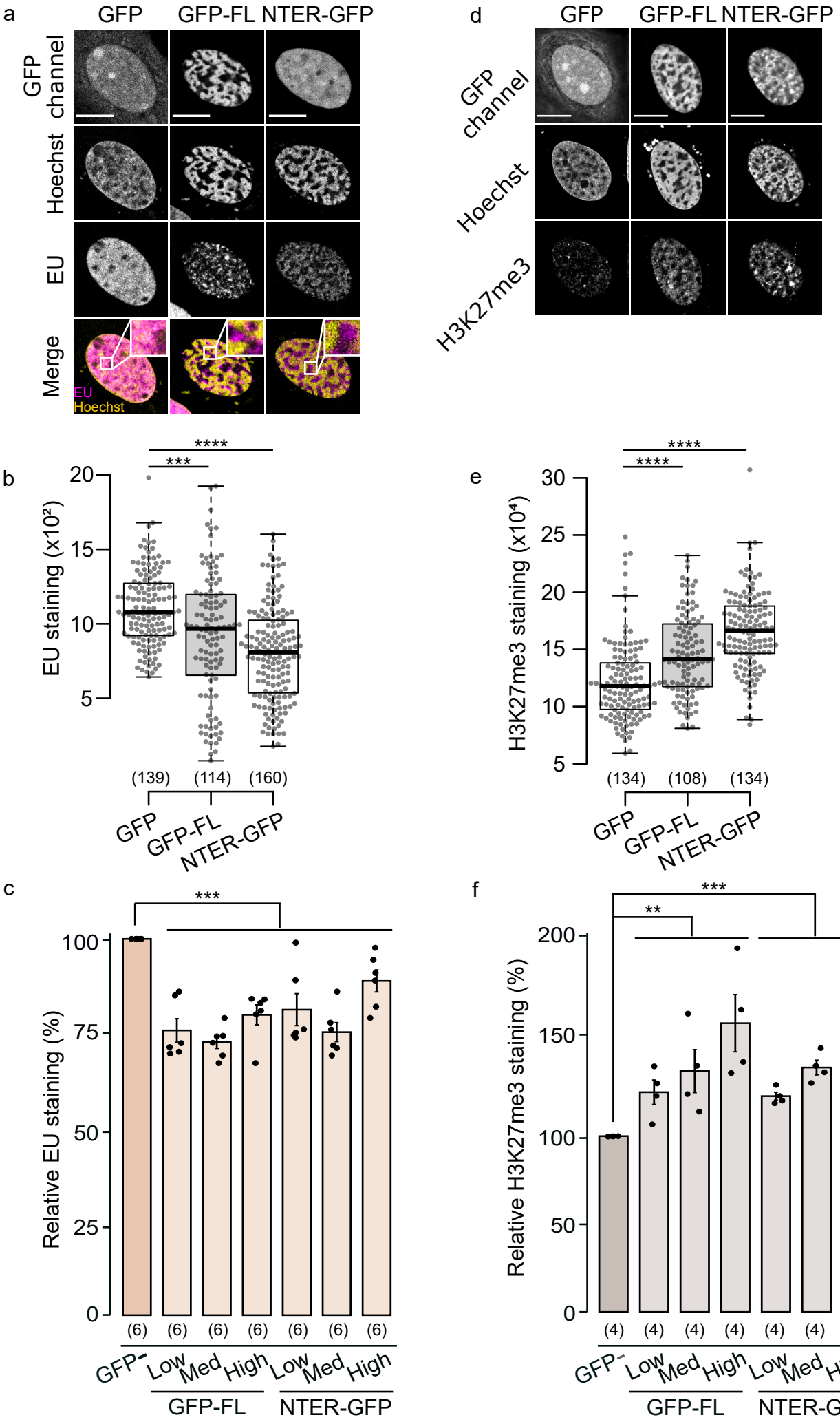

Lejart et al., Figure 4.

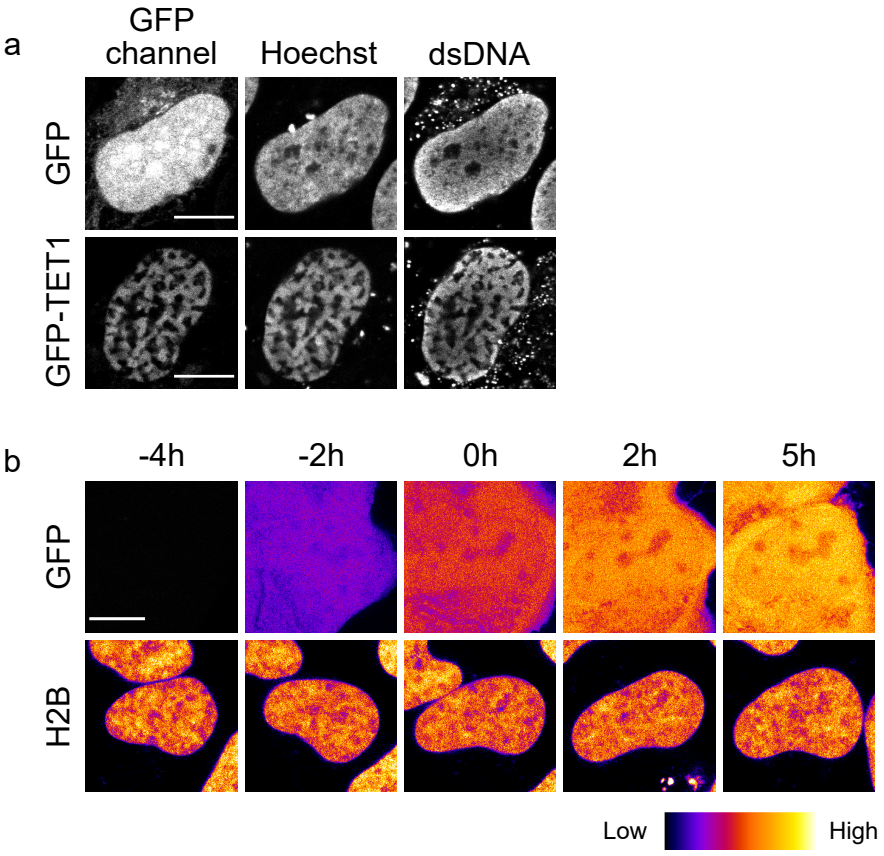

Lejart et al., Supplementary figure1.

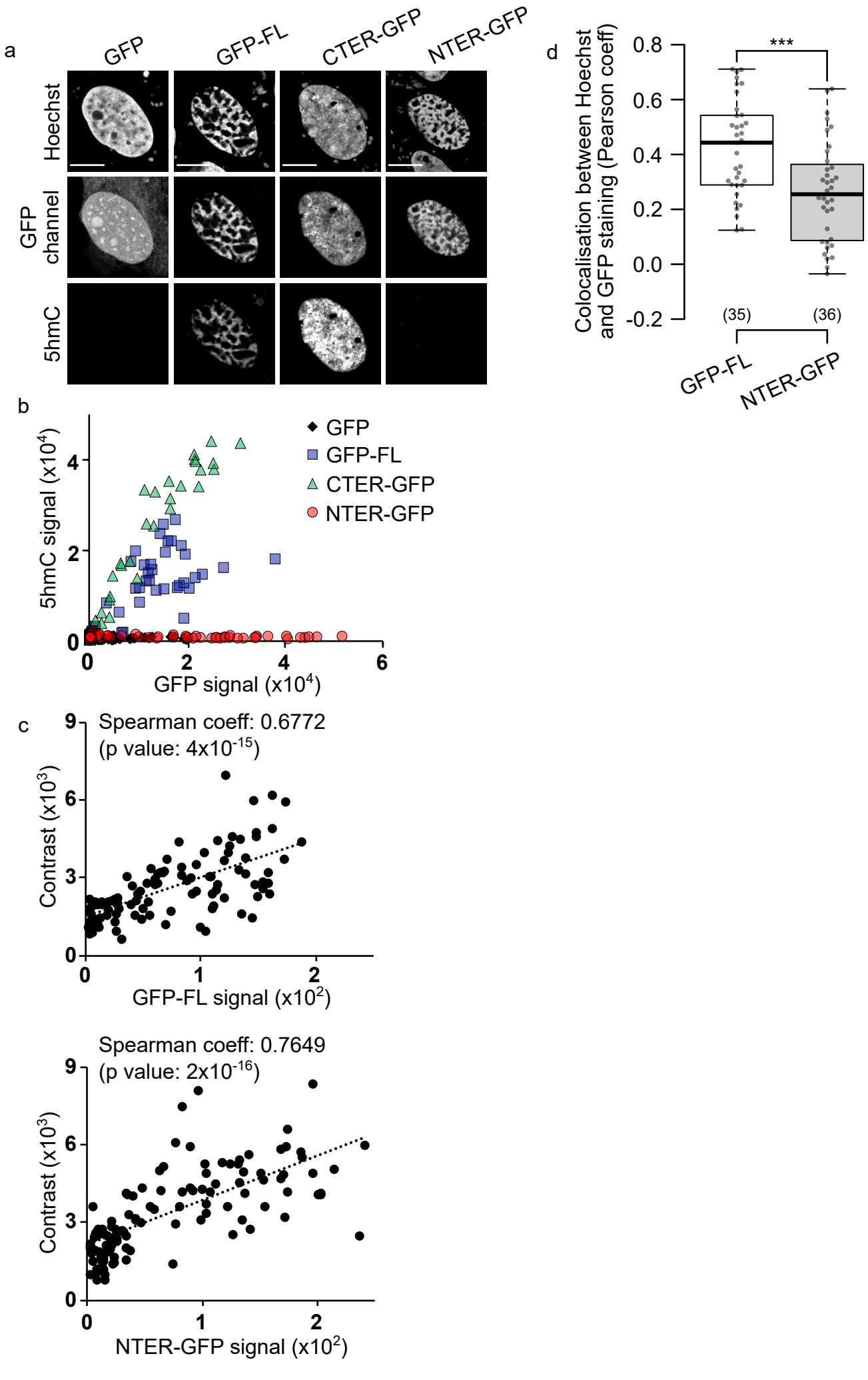

Lejart et al., Supplementary figure 2.

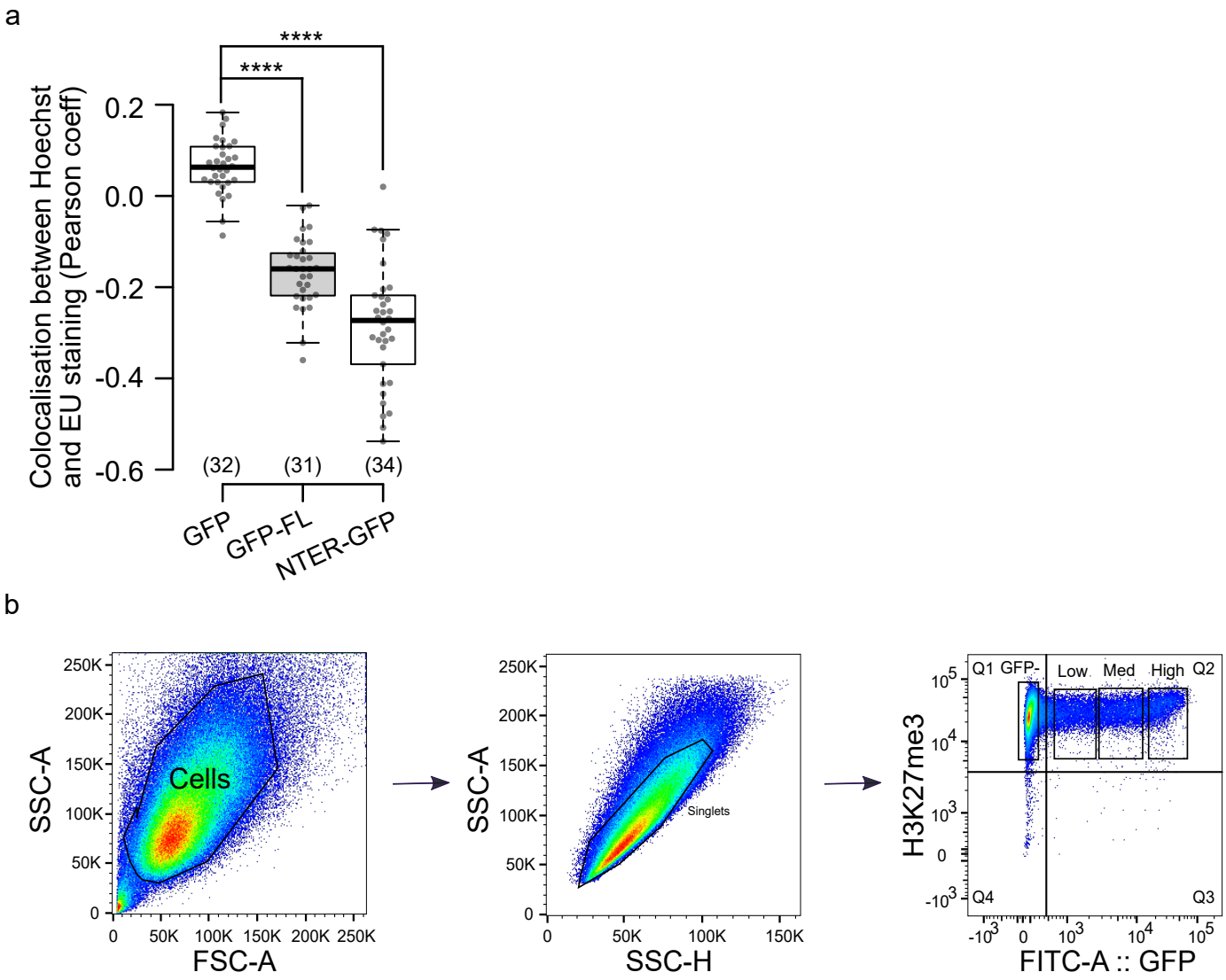

Lejart et al., Supplementary figure 3.